Molecular Inhibition for Selective CO_2 Conversion

Charles E. Creissen,[1] José Guillermo Rivera de la Cruz,[1] Dilan Karapinar,[1] Dario Taverna,[2] Moritz W. Schreiber,[3] Marc Fontecave[1]*

Affiliations

[1] *Laboratoire de Chimie des Processus Biologiques, CNRS UMR 8229, Collège de France, Paris, France*

[2] *Institut de Minéralogie et de Physique des Milieux Condensés, UMR 7590 CNRS, Sorbonne Universités, UPMC Univ Paris 06, 4 place Jussieu, 75005 Paris, France*

[3] *Total Research and Technology, Refining and Chemicals, Division CO_2 Conversion, Feluy, 7181 Seneffe, Belgium*

*Corresponding author. Email: marc.fontecave@college-de-france.fr

Keywords: Electrocatalysis, Molecular Modification, Heterogeneous Catalysis, Carbon Dioxide, Inhibition

Abstract

Electrochemical CO_2 reduction presents a sustainable route to the production of chemicals and fuels. Achieving a narrow product distribution with heterogeneous Cu catalysts is challenging and conventional material modifications offer limited control over selectivity. Here, we show that surface-immobilised molecular species can act as inhibitors for specific carbon products to provide rational control over product

distributions. Combined experimental and computational results showed that anchoring of a thiolfunctionalised pyridine on Cu destabilises a surfacebound reaction intermediate to energetically block a COproducing pathway, thereby favouring formate production. The nitrogen atom was shown to be essential to the inhibition mechanism. The ability of molecules to control selectivity through inhibition of specific reaction pathways offers a unique approach to rationally modify heterogeneous catalysts.

Introduction

Electrochemical CO_2 reduction (CO_2R) demands selective high-rate product generation with low electrical input, which can be facilitated using heterogeneous electrocatalysts.[1–4] Cubased CO_2R catalysts typically generate a wide range of products,[5,6] as selectivity is limited by similar thermodynamic potentials and competing kinetic pathways.[7–9] Catalyst properties such as size, morphology, facet exposure, and density of grain boundaries can be altered to improve product distributions,[10–14] but such modifications often modify multiple properties simultaneously and are convoluted by dynamic changes that can occur under working conditions.[15–17] A proposed alternative route to control selectivity is through the immobilisation of organic molecules that can interact with surfacebound reaction intermediates to promote or obstruct specific reaction pathways.[18–21] These systems would enable the derivation of structureselectivity relationships, providing opportunities for rational design of modified heterogeneous catalysts. However, examples where organic small molecules are directly anchored on Cu catalysts have been precluded by their propensity for desorption under CO_2R conditions.

For CO_2R, Cu surfaces have been functionalised with molecular catalysts,[22] electrodeposited films,[23–25] amino acids,[26] and polymer-based layers,[27,28] but covalent immobilisation of distinct small molecules has proven more difficult. Thiols are capable of forming covalent bonds with Cu surfaces but are susceptible to reductive desorption at the high cathodic potentials generally required for CO_2R.[29,30] This has restricted molecule choice to exclusively long alkyl chains that are retained

close to the surface after desorption due to their high hydrophobicity.[31,32] However, recent developments have shown that alkaline gasfed flow cells are capable of reaching high current densities with low overpotentials.[33,34] We pursued this beneficial characteristic to understand if the mild potentials required to reach high reaction rates could limit reductive desorption of a thiol and provide molecular control over CO_2R selectivity. Here, 4mercaptopyridine (SPy) was immobilised on a Cu catalyst and incorporated in a gas-fed flow cell for high-current density operation (Figure 1a, Figure S1).

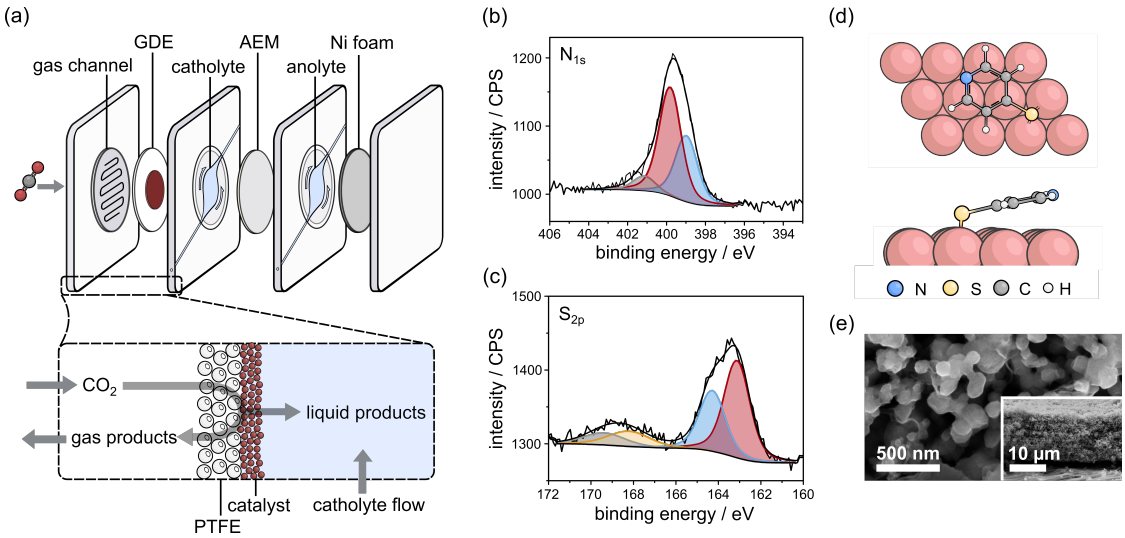

Figure 1. (a) Schematic of the gas fed flow cell setup and components, in which AEM is an anion exchange membrane and GDE is the gas diffusion electrode. The CO_2 is fed through the back of the PTFE layer via the gas channel. (b) and (c) XPS spectra of CuSPy powder showing N_{1s} and S_{2p} environments (background and envelope represented by black lines). (d) Schematic representation of the most stable configuration of 4-mercaptopyridine (SPy) on Cu as determined using DFT calculations. (e) SEM images of the Cu-SPy electrodes.

Results and Discussion

We immobilised SPy on the surface of Cu nanoparticles (NPs) through selfassembly from organic solution. Successful anchoring was initially confirmed using Fourier-transform infrared (FTIR) spectroscopy, which showed signals corresponding to the surfacebound ligand (Figure S2). X-ray photoelectron spectroscopy (XPS) was used to further verify SPy attachment (Figures 1b and 1c, Table S1). The N_{1s} XPS spectrum showed three distinct environments corresponding to protonated and deprotonated

forms of SPy,[35] and the S_{2p} spectrum showed signals arising from physisorbed thiol (164.3 eV) and covalentlybound thiolate (163.1 eV) sulfur environments, alongside small amounts of residual oxidised sulfur (168.2 & 169.4 eV), as expected for this type of immobilisation procedure.[36,37] DFT calculations to determine the optimised conformation of SPy showed that the S preferentially binds two Cu atoms with the ring slightly tilted away from the Cu surface (Figure 1d). Although higher loadings could alter the orientation of SPy, this would simultaneously prevent CO_2 access and therefore limit activity (Figure S3). We observed no obvious differences in morphology or size between bare Cu and Cu-SPy, showing that the modification does not result in surface restructuration (Figure S4).[38] Gas diffusion electrodes (GDEs) were prepared by airbrushing a methanolic solution of ionomer (Nafion) and functionalised CuNPs onto PTFE membranes to form a porous network approximately 10 µm thick (Figure 1e). A geometrical molecular loading of 15 nmol cm^{-2} was determined by UVVis spectroscopy after reductive desorption of SPy at −2.2 V vs. $Ag/AgCl/KCl_{3.4M}$ (Supplementary Note 1).

We observed that higher concentrations of KOH required lower overpotentials for CO_2R at high current density (Figure S5), therefore highly alkaline conditions (5 M KOH) were used to limit SPy desorption. GDEs could reach −500 mA cm^{-2} at applied potentials of approximately −0.5 V vs. RHE with no major differences between the current-voltage responses for Cu and CuSPy samples, showing that the immobilised molecule does not significantly block active sites (Figure 2a, Table S2). Controlled current electrolysis (CCE) experiments conducted at different current densities using Cu and CuSPy showed that the molecular species significantly altered the selectivity. CuSPy GDEs displayed remarkably high faradaic efficiency (FE) values for $HCOO^-$ of (81 ± 4)% at −100 mA cm^{-2} and (72 ± 2)% at −300 mA cm^{-2} with a maximal partial current density for formate of 217 ± 5 mA cm^{-2} and a corresponding cathodic energy efficiency for $HCOO^-$ ($EE_{½\ HCOO^-}$) of (55 ± 3)% (Figure 2b, Table S2). Interestingly, the only other products at −100 mA cm^{-2} were H_2 and CO (Table S2). In contrast, Cu GDEs showed

low FE_{HCOO^-} values and generated a wide range of different products (Figure 2b, Figure S6, Table S2). At −100 mA cm^{-2}, C_{2+} products were observed for the bare Cu catalyst. The FE_{H_2} values were similar for both the bare and modified electrodes, however CuSPy displayed significantly lower yields of CO and C_2H_4, which is formed through CO dimerisation, suggesting that the increase in $HCOO^-$ generation comes at the expense of CO (Figure 2c).[39] The addition of more SPy in the deposition solution did not result in higher FE_{HCOO^-} but also did not decrease activity suggesting that CO_2 access is not limited at these loadings (Figure S7).

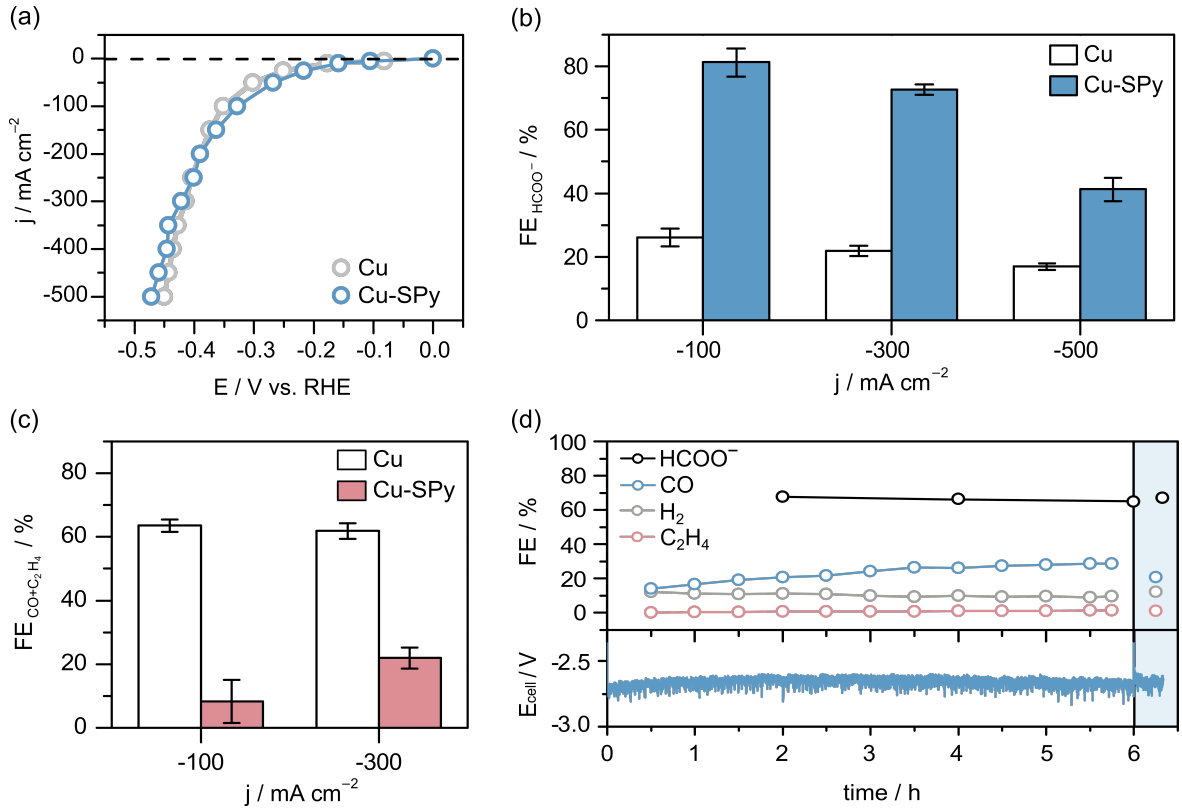

Figure 2. (a) Current-voltage response (iR-corrected) of Cu and Cu-SPy GDEs obtained from chronopotentiometric steps with a 3 min hold time. (b) FE_{HCOO^-} values obtained from controlled current electrolysis (CCE) over 1 h with varying current densities for Cu and Cu-SPy electrodes. (c) $FE_{CO+C_2H_4}$ values for Cu and Cu-SPy electrodes at different current densities. (d) CCE at −300 mA cm^{-2} in a full cell arrangement using a Cu-SPy GDE cathode and a Ni foam anode (no iR correction); the electrolyte solution was replenished after 6 h (shaded blue region represents fresh solution). Error bars represent standard deviation from the mean for triplicate data recorded with fresh electrodes.

At higher current density (−500 mA cm^{-2}) the high formate selectivity was partially lost (FE_{HCOO^-} = (41 ± 4)% after 1h) and the FE_{CO} and $FE_{C_2H_4}$ values increased along with other C_{2+} products (Figures 2b and S5, Table S2). We observed no clear morphological changes following electrolysis that could be responsible for the alteration (Figures S4 and S8). Additionally, the same selectivity trends were observed for metallic nanoparticles (Cu25SPy) that were not exposed to air and therefore did not form an oxide shell prior to catalysis – this suggested that preferential oxide retention was not a factor in selectivity alterations (Table S3). To determine if SPy desorption was responsible for the alteration, we tracked its presence in the electrolyte solution using UVVis spectroscopy (Supplementary Note 1). At −300 mA cm^{-2} (≈ −0.40 V vs. RHE) < 4% desorption was observed after 1 h, and the presence of SPy was confirmed using XPS (Figure S9, Table S4). However, at −500 mA cm^{-2} (≈ −0.45 V vs. RHE) the amount of SPy desorbed from the GDE increased over the course of electrolysis, which correlated well with a drop in $HCOO^-$ selectivity and reached roughly 100% desorption after 2h, confirming that any desorbed species do not remain trapped in the GDE (Figure S10, Table S4). At full molecular desorption, the FE_{HCOO^-} was comparable to that of bare Cu, demonstrating that more cathodic potentials give rise to reductive desorption but also verifying the essential role SPy plays in altering selectivity.

By altering the flow rate of CO_2, we showed that although higher single-pass conversion efficiency (SPCE) values could be obtained, the highest $HCOO^-$ selectivity was observed with a minimum flow rate of 15 mL min^{-1} (SPCE = 14%) (Figure S11). We paired the CuSPy GDE with a Ni foam anode for water oxidation to drive full-cell CO_2R over the course of 6 h. At −300 mA cm^{-2}, a low and stable fullcell potential (E_{cell}) of −2.7 V was obtained with a steady average FE_{HCOO^-} value of approximately 67%, giving a full-cell energy efficiency for $HCOO^-$ of 31% and a SPCE of 14% (Figure 2d). No additional SPy was found in solution throughout electrolysis showing

that the molecule was stable on the surface (Table S4), and replacement of the electrolyte solution after 6 h showed that the high FE_{HCOO^-} was retained (Figure 2d), thereby ruling out contributions from solution-dissolved species.

Having established enhanced $HCOO^-$ production with CuSPy, we used two thiols with different structural features to help understand the mechanism. We first immobilised thiophenol (SPh), which is structurally similar to SPy but lacks the nitrogen functionality, and conducted CCE experiments under the same conditions as for Cu-SPy. We observed that CuSPh GDEs showed comparable $HCOO^-$ selectivity to unmodified Cu electrodes (Table S3) – this suggested that the nitrogen plays a key role in favouring formate production. We next studied the nitrogen contribution by looking into the possibility that reduced pyridine could act as a hydride donor. In highly alkaline conditions at cathodic potentials, dihydropyridine formation is only possible at the 2 or 6 positions of the pyridine.[40] Therefore we synthesised 2,6-dimethyl-4mercaptopyridine (DMSPy), for which these sites are blocked, to see if the selectivity was altered. At −300 mA cm^{-2} we observed similar $HCOO^-$ yields to Cu-SPy, and consequently showed that a pyridine-based hydride mechanism was not possible, in line with previous works (Table S3).[41,42] These experiments showed that the nitrogen plays an important role but its exact function was unclear. We used DFT calculations to identify possible alterations that could account for the selectivity enhancement.

DFT calculations identified three main pathways involving different reaction intermediates in the formation of CO and HCOOH in agreement with previous studies (Figure 3a, Figure S14).[9,43,44] The first proton-coupled electron transfer produces two surface-adsorbed intermediates that generate CO, which are labelled *OCOH and *OCOH', as well as one intermediate that produces HCOOH, labelled *COOH (Figure S15). We performed calculations on each CO_2 reduction and hydrogen evolution pathways in the presence and absence of SPy (Figures S16-S22). There was no alteration to the

free energy profile for *H, the surface-adsorbed hydrogen intermediate, showing that the molecule does not stabilise hydrogen on the surface; this also supports the experimental results which showed an unaltered FE_{H_2} with Cu-SPy (Figure S23).

Interestingly, the formate pathway showed only minimal free energy changes, as did one of the CO-generating pathways (involving *OCOH') (Figures S24-S25). However, the CO pathway involving *OCOH showed significant increases in the free energies of both the $*CO_2^-$ and *OCOH intermediates in the presence of SPy – this thermodynamically prevents CO formation through the *OCOH pathway (Figures 3a and 3b, Figure S26). Electron density difference plots identified a destabilising interaction that would occur between the N atom of the SPy and the surface-bound intermediate (Figure 3c). This accounts for the increase in free energy, which prevents the formation of *OCOH when SPy is immobilised on the surface. As a consequence, the *OCOH-SPy interaction cannot be observed using spectroscopic techniques. The molecular inhibition mechanism agrees with the described experimental observations that formate production comes at the expense of CO and C_{2+} products, which are derived from CO-CO dimerisation.[9,39] Thus, by preventing CO generation, the surface-bound SPy directs selectivity towards formate.

Conclusion

The system presented herein shows that modification of a Cu catalyst with a distinct molecular species enhances high-rate CO_2R selectivity by inhibiting production of a specific carbon product. The immobilisation of 4-mercaptopyridine on the surface of Cu energetically blocks the formation of intermediates involved in the generation of CO, thereby facilitating selective formate production. We highlighted an advantage of molecular modification by the incorporation of different structures to identify that nitrogen was key to the mechanism, allowing DFT calculations to explore the interactions responsible for inhibition, which supported experimentally observed

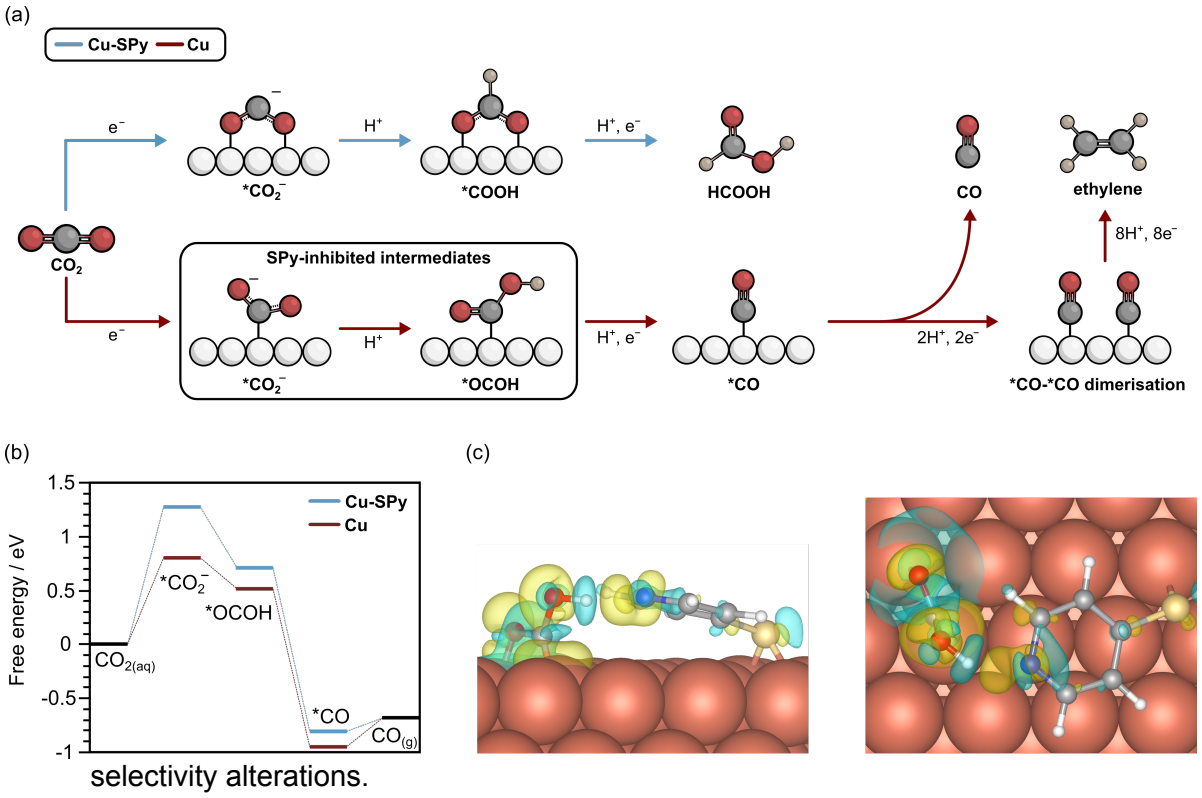

selectivity alterations.

Figure 3. (a) Reaction pathways towards CO and C_{2+} products (red, Cu) or HCOOH (blue, CuSPy) showing the inhibited intermediates. The *OCOH' intermediate has been omitted for clarity as SPy does not alter this pathway. (b) Reaction free energy profiles for CO_2 reduction to CO on Cu and CuSPy surfaces at −0.4 V vs. RHE. (c) charge density difference plots showing that the presence of SPy energetically blocks the formation of *OCOH, where blue lobes correspond to depletion and yellow lobes

The drastic change in selectivity due to the immobilisation of a simple molecule incentivises the exploration of more complex functional groups to block or promote intermediates involved in the generation of multicarbon products in future work. Molecular inhibition therefore offers an adaptable route to direct selectivity in catalytic reactions.

References

[1] P. De Luna, C. Hahn, D. Higgins, S. A. Jaffer, T. F. Jaramillo, E. H. Sargent, *Science* **2019**, *364*, eaav3506.

[2] D. Karapinar, C. E. Creissen, J. G. Rivera de la Cruz, M. W. Schreiber, M. Fontecave,

ACS Energy Lett. **2021**, *6*, 694–706.

[3] Y. Y. Birdja, E. Pérez-Gallent, M. C. Figueiredo, A. J. Göttle, F. Calle-Vallejo, M. T. M. Koper, *Nat. Energy* **2019**, *4*, 732–745.

[4] C. E. Creissen, M. Fontecave, *Adv. Energy Mater.* **2021**, *11*, 2002652.

[5] S. Nitopi, E. Bertheussen, S. B. Scott, X. Liu, A. K. Engstfeld, S. Horch, B. Seger, I. E. L. Stephens, K. Chan, C. Hahn, J. K. Nørskov, T. F. Jaramillo, I. Chorkendorff, *Chem. Rev.* **2019**, *119*, 7610–7672.

[6] Y. Hori, I. Takahashi, O. Koga, N. Hoshi, *J. Phys. Chem. B* **2002**, *106*, 15–17.

[7] Z. W. Seh, J. Kibsgaard, C. F. Dickens, I. Chorkendorff, J. K. Nørskov, T. F. Jaramillo, *Science* **2017**, *355*, eaad4998.

[8] A. A. Peterson, J. K. Nørskov, *J. Phys. Chem. Lett.* **2012**, *3*, 251–258.

[9] T. K. Todorova, M. W. Schreiber, M. Fontecave, *ACS Catal.* **2020**, *10*, 1754–1768.

[10] P. De Luna, R. Quintero-Bermudez, C. T. DInh, M. B. Ross, O. S. Bushuyev, P. Todorović, T. Regier, S. O. Kelley, P. Yang, E. H. Sargent, *Nat. Catal.* **2018**, *1*, 103–110.

[11] A. Loiudice, P. Lobaccaro, E. A. Kamali, T. Thao, B. H. Huang, J. W. Ager, R. Buonsanti, *Angew. Chem. Int. Ed.* **2016**, *55*, 5789–5792.

[12] K. Jiang, R. B. Sandberg, A. J. Akey, X. Liu, D. C. Bell, J. K. Nørskov, K. Chan, H. Wang, *Nat. Catal.* **2018**, *1*, 111–119.

[13] Y. Wang, Z. Wang, C. T. Dinh, J. Li, A. Ozden, M. Golam Kibria, A. Seifitokaldani, C. S. Tan, C. M. Gabardo, M. Luo, H. Zhou, F. Li, Y. Lum, C. McCallum, Y. Xu, M. Liu, A. Proppe, A. Johnston, P. Todorovic, T. T. Zhuang, D. Sinton, S. O. Kelley, E. H. Sargent, *Nat. Catal.* **2020**, *3*, 98–106.

[14] R. G. Mariano, K. McKelvey, H. S. White, M. W. Kanan, *Science* **2017**, *358*, 1187–1192.

[15] J. Vavra, T. H. Shen, D. Stoian, V. Tileli, R. Buonsanti, *Angew. Chem. Int. Ed.* **2021**, *60*, 1347–1354.

[16] R. M. Arán-Ais, R. Rizo, P. Grosse, G. Algara-Siller, K. Dembélé, M. Plodinec, T. Lunkenbein, S. W. Chee, B. R. Cuenya, *Nat. Commun.* **2020**, *11*, 3489.

[17] J. Huang, N. Hörmann, E. Oveisi, A. Loiudice, G. L. De Gregorio, O. Andreussi, N. Marzari, R. Buonsanti, *Nat. Commun.* **2018**, *9*, 3117.

[18] A. Wagner, C. D. Sahm, E. Reisner, *Nat. Catal.* **2020**, *3*, 775–786.

[19] D. H. Nam, P. De Luna, A. Rosas-Hernández, A. Thevenon, F. Li, T. Agapie, J. C. Peters, O. Shekhah, M. Eddaoudi, E. H. Sargent, *Nat. Mater.* **2020**, *19*, 266–276.

[20] Y. Fang, J. C. Flake, *J. Am. Chem. Soc.* **2017**, *139*, 3399–3405.

[21] Q. Zhu, C. J. Murphy, L. R. Baker, *J. Am. Chem. Soc.* **2022**, *144*, 2829–2840.

[22] F. Li, Y. C. Li, Z. Wang, J. Li, D. H. Nam, Y. Lum, M. Luo, X. Wang, A. Ozden, S. F. Hung, B. Chen, Y. Wang, J. Wicks, Y. Xu, Y. Li, C. M. Gabardo, C. T. Dinh, Y. Wang, T. T. Zhuang, D. Sinton, E. H. Sargent, *Nat. Catal.* **2020**, *3*, 75–82.

[23] Z. Han, R. Kortlever, H. Y. Chen, J. C. Peters, T. Agapie, *ACS Cent. Sci.* **2017**, *3*, 853–859.

[24] F. Li, A. Thevenon, A. Rosas-Hernández, Z. Wang, Y. Li, C. M. Gabardo, A. Ozden, C. T. Dinh, J. Li, Y. Wang, J. P. Edwards, Y. Xu, C. McCallum, L. Tao, Z. Q. Liang, M. Luo, X. Wang, H. Li, C. P. O'Brien, C. S. Tan, D. H. Nam, R. Quintero-Bermudez, T. T. Zhuang, Y. C. Li, Z. Han, R. D. Britt, D. Sinton, T. Agapie, J. C. Peters, E. H. Sargent, *Nature* **2020**, *577*, 509–513.

[25] T. T. H. Hoang, S. Ma, J. I. Gold, P. J. A. Kenis, A. A. Gewirth, *ACS Catal.* **2017**, *7*, 3313–3321.

[26] M. S. Xie, B. Y. Xia, Y. Li, Y. Yan, Y. Yang, Q. Sun, S. H. Chan, A. Fisher, X. Wang, *Energy Environ. Sci.* **2016**, *9*, 1687–1695.

[27] X. Chen, J. Chen, N. M. Alghoraibi, D. A. Henckel, R. Zhang, U. O. Nwabara, K. E. Madsen, P. J. A. Kenis, S. C. Zimmerman, A. A. Gewirth, *Nat. Catal.* **2021**, *4*, 20–27.

[28] S. Ahn, K. Klyukin, R. J. Wakeham, J. A. Rudd, A. R. Lewis, S. Alexander, F. Carla, V. Alexandrov, E. Andreoli, *ACS Catal.* **2018**, *8*, 4132–4142.

[29] J. R. Pankhurst, P. Iyengar, A. Loiudice, M. Mensi, R. Buonsanti, *Chem. Sci.* **2020**, *11*, 9296–9302.

[30] J. C. Love, L. A. Estroff, J. K. Kriebel, R. G. Nuzzo, G. M. Whitesides, *Chem. Rev.* **2005**, *105*, 1103–1169.

[31] D. Wakerley, S. Lamaison, F. Ozanam, N. Menguy, D. Mercier, P. Marcus, M. Fontecave, V. Mougel, *Nat. Mater.* **2019**, *18*, 1222–1227.

[32] D. Kim, S. Yu, F. Zheng, I. Roh, Y. Li, S. Louisia, Z. Qi, G. A. Somorjai, H. Frei, L. W. Wang, P. Yang, *Nat. Energy* **2020**, *5*, 1032–1042.

[33] F. P. García de Arquer, C. T. Dinh, A. Ozden, J. Wicks, C. McCallum, A. R. Kirmani, D. H. Nam, C. Gabardo, A. Seifitokaldani, X. Wang, Y. C. Li, F. Li, J. Edwards, L. J. Richter, S. J. Thorpe, D. Sinton, E. H. Sargent, *Science* **2020**, *367*, 661–666.

[34] M. Zhong, K. Tran, Y. Min, C. Wang, Z. Wang, C. T. Dinh, P. De Luna, Z. Yu, A. S. Rasouli, P. Brodersen, S. Sun, O. Voznyy, C. S. Tan, M. Askerka, F. Che, M. Liu, A. Seifitokaldani, Y. Pang, S. C. Lo, A. Ip, Z. Ulissi, E. H. Sargent, *Nature* **2020**, *581*, 178–183.

[35] S. Herrera, F. Tasca, F. J. Williams, E. J. Calvo, P. Carro, R. C. Salvarezza, *Langmuir* **2017**, *33*, 9565–9572.

[36] D. G. Castner, K. Hinds, D. W. Grainger, *Langmuir* **1996**, *12*, 5083–5086.

[37] Y. Wang, J. Im, J. W. Soares, D. M. Steeves, J. E. Whitten, *Langmuir* **2016**, *32*, 3848–3857.

[38] A. Thevenon, A. Rosas-Hernández, J. C. Peters, T. Agapie, *Angew. Chem. Int. Ed.* **2019**, *58*, 16952–16958.

[39] J. H. Montoya, C. Shi, K. Chan, J. K. Nørskov, *J. Phys. Chem. Lett.* **2015**, *6*, 2032–2037.

[40] J. A. Keith, E. A. Carter, *Chem. Sci.* **2013**, *4*, 1490–1496.

[41] C. Costentin, J. M. Savéant, C. Tard, *ACS Energy Lett.* **2018**, *3*, 695–703.

[42] M. Dunwell, Y. Yan, B. Xu, *ACS Catal.* **2017**, *7*, 5410–5419.

[43] R. Kortlever, J. Shen, K. J. P. Schouten, F. Calle-Vallejo, M. T. M. Koper, *J. Phys. Chem. Lett.* **2015**, *6*, 4073–4082.

[44] R. García-Muelas, F. Dattila, T. Shinagawa, A. J. Martín, J. Pérez-Ramírez, N. López, *J. Phys. Chem. Lett.* **2018**, *9*, 7153–7159.

Acknowledgements

This work was supported financially by funding from Total Research & Technology Feluy. This work was granted access to the HPC/AI resources of TGCC under the allocation 2020-A0090811911 made by GENCI. We thank Arnaud Etcheberry, Mathieu Fregnaux, and Muriel Bouttemy for XPS measurements, and Françoise Pillier for SEM analysis. The datasets generated during and/or analysed during the current study are available from the corresponding author on reasonable request.

Competing Interests: A provisional European patent application for this work (EP21315179.8) was filed on the 24th of September 2021 in the joint names of Total SE and Collège de France.

Supporting Information:

Materials and Methods

Computational Methods and Models

Supplementary Figures and Notes

Supplementary Tables S1 – S6

Supplementary References

Correspondence and requests for materials should be addressed to

marc.fontecave@college-de-france.fr

Table of Contents:

Molecular modifiers can be used to alter the product selectivity of heterogeneous catalysts for electrochemical carbon dioxide reduction. In this study, we showed that immobilisation of a well-defined pyridine species on a copper catalyst inhibits CO and C_{2+} product formation, enabling the selective generation of formate at high reaction rates.